

Synthesis of nanoscale SmFe intermetallic phases by a reduction-diffusion process of a powder mixture of Sm₂O₃-CaH₂-Fe

Joon-Chul Yun and Jai-Sung Lee*

Department of Metallurgy and Materials Science, Hanyang University-ERICA campus, Ansan 426-791, Korea

This study investigates the synthesis of SmFe intermetallic compounds by a solid state reduction-diffusion process (R-D process) using a mixture of Sm₂O₃-CaH₂ ball-milled powders and Fe nanopowders. The Sm₂O₃-CaH₂-Fe mixed powders were subjected to heat treatment under a switched gas atmosphere from Ar-5 vol.%H₂ to a vacuum atmosphere during the R-D process at 800 °C. It was found that the SmFe intermetallic phases of Sm₂Fe₁₇ and SmFe₃ were effectively formed in a switched gas atmosphere and observed on the surface of the sintered Fe nanopowder agglomerate. This formation occurred because the sintering of agglomerated Fe nanopowders occurred at a low temperature of about 500 °C earlier before the Sm dissociated from SmH₂ was diffused into the sintered Fe nanopowders agglomerate during the R-D process. The Sm₂Fe₁₇ phase of the target alloy was identified having a rhombohedral Th₂Zn₁₇-type (2:17 R) structure with a grain size of 400-800 nm. It is expected that the Sm₂Fe₁₇ nanopowders can be effectively fabricated by controlling the initial powder characteristics such as size refinement and mixing homogeneity.

Key words: Samarium oxide, Intermetallic compounds, Nanocrystalline, Reduction-diffusion process, Permanent magnets, Microstructure, Powder metallurgy.

Introduction

Samarium-iron nitride (Sm₂Fe₁₇N_x) is a promising hard magnetic material [1, 2] which is generally utilized in the form of a resin-bonded magnet because Sm₂Fe₁₇N_x powders are hardly sintered near the Curie temperature (470 °C). Moreover, low thermal stability leading to decomposition of the Sm₂Fe₁₇N_x phase into SmN and the α-Fe phase at elevated temperature is another key factor for a lack of sintered Sm₂Fe₁₇N_x hard magnets [3]. For this reason much effort is being paid to fabrication of sintered Sm₂Fe₁₇N₃ powder by pressure-assisted sintering methods [4, 5]. However, the results have not been satisfactory due to the low sinterability of micro powders as well as pressure-induced phase decomposition. In general, Sm₂Fe₁₇N_x powder is produced in two ways; one is pulverization and nitrogenation of Sm₂Fe₁₇ ingot material [6] and the other is reduction of Sm₂O₃ into Sm by liquid Ca and a diffusion reaction with Fe and finally nitrogenation of Sm₂Fe₁₇ [2, 7, 8]. However, both processes are restricted to fabricating nanosized Sm₂Fe₁₇ powder due to the high-temperature process above 1000 °C which induces remarkable grain growth. To override this limitation, therefore, the authors suggest a low temperature solid state reduction-diffusion process (R-D process) for fabricating nanoscale Sm₂Fe₁₇ powder by using a Sm₂O₃-CaH₂-Fe mixed powder as

well as reducing diffusion paths during alloying. In our previous work [9] we found that Sm₂Fe₁₇ intermetallics were possibly manufactured by this process, in which the Sm₂Fe₁₇ phase was formed by the inter-diffusion reaction between Fe and Sm where the Sm is generated by decomposition of SmH₂ under various conditions. This experimental finding provides an important implication that such a low temperature reaction of the SmFe phase enables us to fabricate a very fine intermetallic phase depending on process conditions. In order to verify this idea experimentally, we investigated the formation of a nanocrystalline Sm₂Fe₁₇ intermetallic phase by a solid state R-D process for a mixture of nanosized Sm₂O₃-CaH₂-Fe below the melting point of CaH₂. The results are discussed in terms of the microstructure and phase analysis.

Experimental

The starting materials were samarium oxide powder (Sm₂O₃, 99.9% purity, 1 μm in average particle size), calcium hydride flake powder (CaH₂, 94% purity) and iron nanopowder (150 nm in average particle size). The iron nanopowders were prepared by hydrogen reduction of ball-milled iron oxide powders (Fe₂O₃, 99.9% purity) [10]. The experimental procedure is schematically represented in Fig. 1. First, the Sm₂O₃-CaH₂ powder mixture was prepared by ball-milling using SPEX mill (Spex Industries 8000 M Spex Mixer/Mill) at a speed of 1060 revolutions/minute for 1 h. The oxide mixture was composed of 1.1 for Sm₂O₃ and 4.5 for CaH₂ times

*Corresponding author:
Tel : +82-31-400-5225
Fax: +82-31-406-5170
E-mail: jslee@hanyang.ac.kr

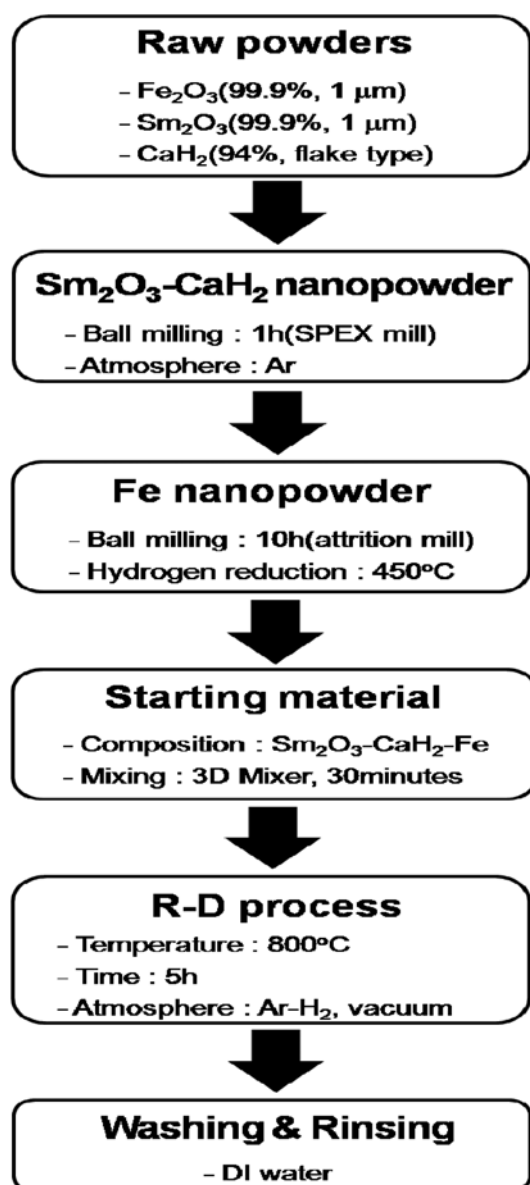


Fig. 1. Schematic diagram of experimental procedure.

the chemical equivalent in excess of stoichiometry to compensate for their loss during R-D process in an argon atmosphere [8]. The ball-milled oxide powders were then mixed with Fe nanopowders using a tubular mixer for 30 minutes. All experimental procedures for preparing the starting material of $\text{Sm}_2\text{O}_3\text{-CaH}_2\text{-Fe}$ powders were conducted in an argon (99.999%)-filled glove box in order to prevent re-oxidation of the Fe nanopowder and phase change in CaH_2 .

The annealing for the solid state R-D process was carefully performed to avoid a phase change during the entire annealing process. For this, the powders were put in a stainless steel container box ($50 \times 50 \times 30$ mm) with a covering lid to prevent the evaporation loss of Sm_2O_3 and CaH_2 during reaction. Then the container was heated up to 800°C at a rate of 5Kminute^{-1} in a mixed gas of Ar-5 vol.\%H_2 and isothermally held for

5 h. The isothermal annealing was conducted in a stepwise way by switching the gas atmosphere from the mixed gas to a vacuum (1 Pa). Namely, the atmosphere switching was carried out after 3 h annealing in the mixed gas to 2 h annealing in vacuum. After isothermal annealing, the powders were cooled in a vacuum to room temperature.

The R-D processed powders were recovered by washing the product several times with DI water to remove CaO [7]. A phase analysis of the powders was conducted by X-ray diffraction (XRD, RIGAKU D/MAX-2500/PC) using a $\text{CuK}\alpha$ target at a scanning speed of $4^\circ\text{minute}^{-1}$. The powder morphology and cross section were examined by scanning electron microscopy (SEM, HITACHI S-4800). The elemental compositions of the powder were analyzed by energy dispersive X-ray spectroscopy (EDS, HORIBA EMAX mics). In order to investigate the crystal structure of SmFe phase, a TEM specimen was prepared from the cross section of the SmFe phase in the annealed powders using a focused ion beam (FIB, TESCAN LYRA FEG1) technique. The FIB was operated at an accelerating voltage of 30 kV and a 40 pA beam for fine milling. The specimen was observed by transmission electron microscopy (TEM, JEOL J-2010), and selected area diffraction studies were used to identify the crystal structure of the SmFe intermetallic phases.

Results and discussion

Powder characteristics

Fig. 2a, b show SEM micrographs of Fe nanopowders and of ball-milled $\text{Sm}_2\text{O}_3\text{-CaH}_2$ powders. It is seen that the particle sizes of both powders are about 150 nm for Fe powders and several tens of nanometer for $\text{Sm}_2\text{O}_3\text{-CaH}_2$ mixed powders, respectively. The morphology of $\text{Sm}_2\text{O}_3\text{-CaH}_2\text{-Fe}$ powders after mixing is depicted in Fig. 2c and shows an agglomerated form with a wide size distribution of 5-50 μm . In general, the completeness of the R-D process strongly depends on the initial particle size of the powders [8]. Therefore, the finer the particle size such as nanosized particles becomes, the lower the reaction temperature and the shorter the reaction time required. Phase analysis by an XRD pattern in Fig. 2d reveals that this powder is composed of Sm_2O_3 , Fe and CaH_2 phases. Generally, CaH_2 is very sensitive to a phase change into the Ca(OH)_2 phase under atmospheric conditions [11]. In this sense, the absence of Ca(OH)_2 phase in the mixed powder as shown in Fig. 2d confirms that the preparation of the $\text{Sm}_2\text{O}_3\text{-CaH}_2\text{-Fe}$ powders was satisfactorily conducted by fulfilling the requirements of particle refinement, homogeneous mixing and no phase change.

Reduction-Diffusion process

Fig. 3 shows the XRD patterns of the powder samples after the R-D process by annealing at 800°C

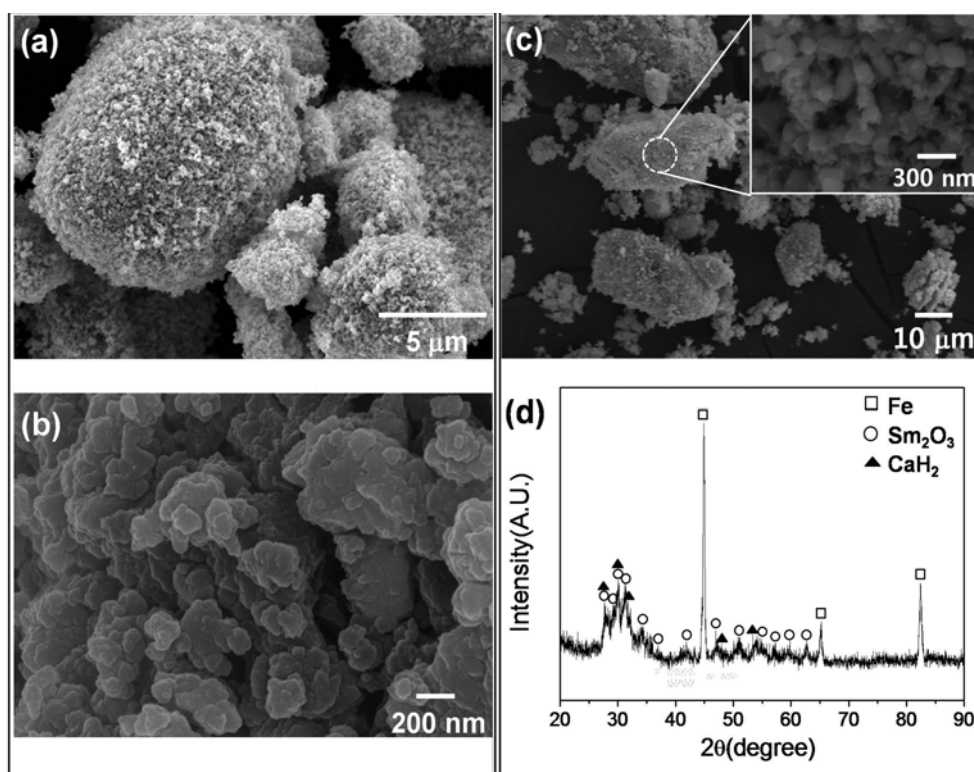


Fig. 2. Microstructures and XRD pattern of the starting materials: (a) hydrogen reduced Fe nanopowders, (b) ball-milled $\text{Sm}_2\text{O}_3\text{-CaH}_2$ powders and (c) $\text{Sm}_2\text{O}_3\text{-CaH}_2\text{-Fe}$ mixed powders.

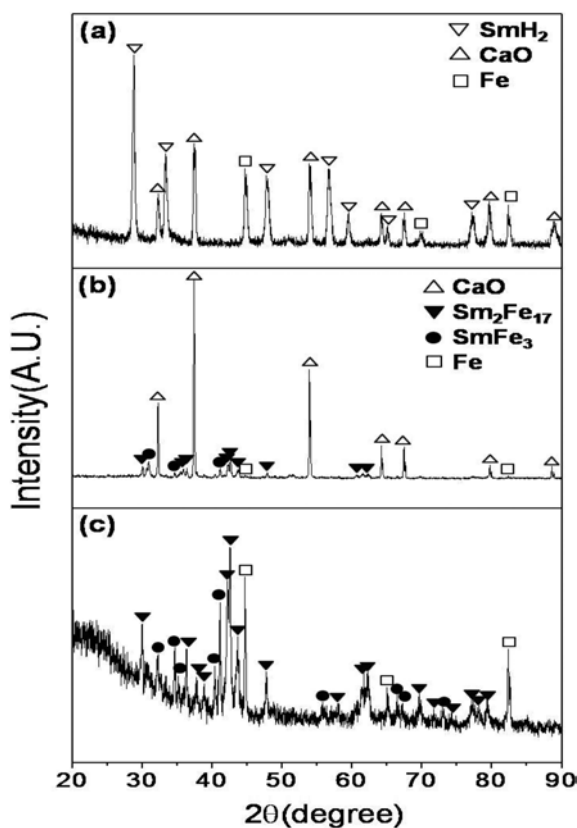


Fig. 3. XRD patterns of the R-D processed $\text{Sm}_2\text{O}_3\text{-CaH}_2\text{-Fe}$ mixed powders in (a) Ar-5 vol.% H_2 and (b, c) switched gas atmosphere from Ar-5 vol.% H_2 to vacuum. *(c) after a washing treatment in water.

in two different atmospheres: one is in Ar-5 vol.% H_2 (Fig. 3a) and the other in a switched atmosphere from Ar-5 vol.% H_2 to a vacuum (Fig. 3b, c). In the former case, there are only three peaks for SmH_2 , CaO and Fe except for the intermetallic phases. In particular, the presence of SmH_2 and CaO indicates that the Sm_2O_3 phase was completely reduced by the Ca decomposed from CaH_2 . It is reported that the SmH_2 phase starts to form by a reaction between the samarium and hydrogen molecules at 600 °C in which both Sm and H_2 are generated by two previous reactions of the decomposition into Ca and H_2 and the subsequent reduction of Sm_2O_3 by decomposed Ca [7, 9]. However, the presence of the SmH_2 and Fe phases also imply that the decomposition of SmH_2 into Sm did not occur and, as a consequence, the Fe could not participate in the diffusion reaction for the formation of the SmFe intermetallic phase. This phenomenon is intuitively attributed to the low hydrogen content of Ar-5 vol.% H_2 . The low hydrogen content atmosphere not only enhanced the hydration of reduced Sm atoms into SmH_2 but also suppressed the decomposition of the SmH_2 . According to the equilibrium phase diagram of the Sm-H system [12], the SmH_2 phase exists as an equilibrium ϵ phase at 800 °C which undergoes reversible reactions of formation and decomposition depending on the temperature and hydrogen pressure. The higher the H_2 partial pressure and the lower the reaction temperature are the more stable the SmH_2 becomes. The SmH_2 is decomposed more favorably

with decreasing H_2 pressure or increasing temperature [12, 13]. In this respect, it seems that the Ar-5 vol.% H_2 atmosphere in this study has a high hydrogen activity so as to suppress the decomposition of the SmH_2 phase and the subsequent diffusion reaction for the formation of the SmFe intermetallics. Regarding the temperature effect, it has been reported that recombination of Sm_2Fe_{17} phase from SmH_2 occurs near 1000 °C in H_2 [14] and above 950 °C in an Ar-5 vol.% H_2 atmosphere [9]. However, such a high temperature reaction induces particle coarsening which is not appropriate for producing a fine structured intermetallic phase. For this reason, it seems reasonable that the use of a switching atmosphere is selected to control the microstructure of SmFe intermetallics during a low temperature reaction.

In order to enhance the decomposition of the SmH_2 , the Ar-5 vol.% H_2 gas atmosphere was switched to a vacuum atmosphere (1 Pa) during the isothermal annealing. As a result, the two intermetallic phases of Sm_2Fe_{17} and $SmFe_3$ together with residual Fe and CaO were formed as seen in Fig. 3b. This result also shows residual Fe and CaO. It is recognized that those intermetallic phases could be effectively formed by a diffusion reaction between Sm and Fe which is easily decomposed from SmH_2 in a vacuum atmosphere [14]. In particular, the Sm_2Fe_{17} phase of the final target intermetallic phase in this study is identified as a rhombohedral Th_2Zn_{17} -type (2:17 R) crystal structure, which is the normal crystal structure of the conventional polycrystalline Sm_2Fe_{17} alloy in an equilibrium state [15]. This result offers a very important breakthrough for the creation of SmFe intermetallic compounds by a solid state reaction. To confirm this result more clearly, the phase analysis was conducted for the same sample

after removing CaO by washing with water. It is seen from the XRD pattern of Fig. 2c that the powder sample is composed of Sm_2Fe_{17} , $SmFe_3$ and a residual Fe phase. To our knowledge, this is the first experimental finding of a Sm_2Fe_{17} phase formed by the R-D process at a low temperature of 800 °C.

Microstructure and phase analysis

Fig. 4 presents the SEM micrographs and EDS spectra for the powder sample (the same as the sample in Fig. 3c). It is seen in Fig. 4a that the large powder sample is about 100 μm in size and has a porous surface. The cross section of the powder in Fig. 4b reveals three different phases (denoting 'A', 'B', and 'C') in the form of a core-layer structure and discrete located pores along the interfaces. The EDS analysis of Fig. 4c confirms that the atomic ratios of Sm to Fe of two surface layers are 1:3.3 (spectrum A) and 1:8.9 (spectrum B). According to the Sm-Fe equilibrium phase diagram [16], those layer phases correspond to the intermetallic phases of $SmFe_3$ and Sm_2Fe_{17} , respectively. Also, the spectrum C discloses that the center zone of the powder consists of a pure Fe phase. It is known that these intermetallic phases are formed by an inter-diffusion process between Sm and Fe, especially in which fast diffusion of Sm atoms into Fe plays a dominant role in the diffusion process [17]. The microstructure shows that the Fe phase mostly remains unreacted, while the Sm is completely consumed for the formation of the intermetallic phases. This microstructural phenomenon confirms that the Sm atom is a fast diffuser in the diffusion reaction and also the annealing condition has not yet reached an equilibrium state for the formation of Sm_2Fe_{17} .

From the kinetic point-of-view, the kinetics of the

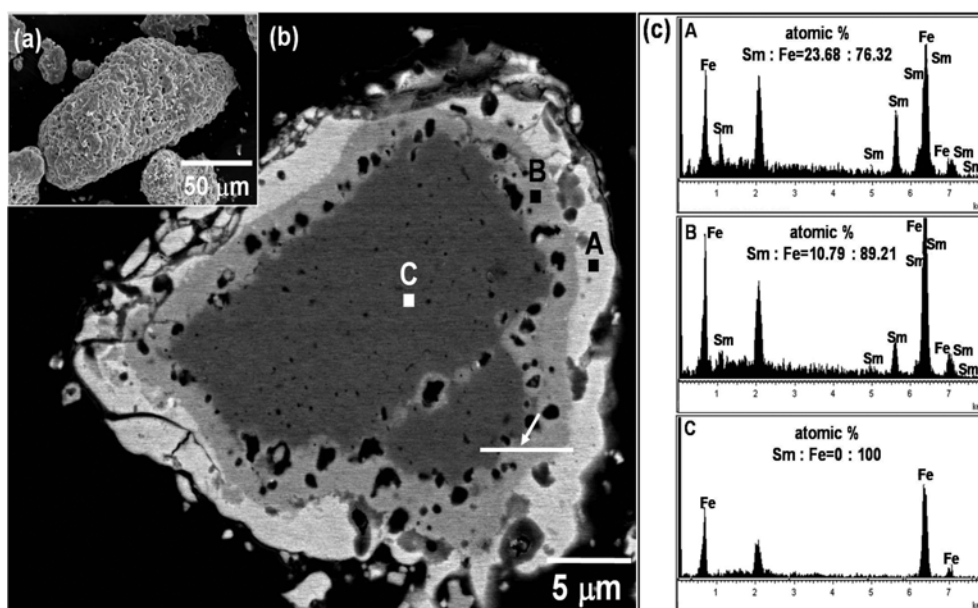


Fig. 4. SEM micrographs and EDS spectra of R-D processed powder after the washing process: (a) surface morphology, (b) cross section, and (c) EDS spectra.

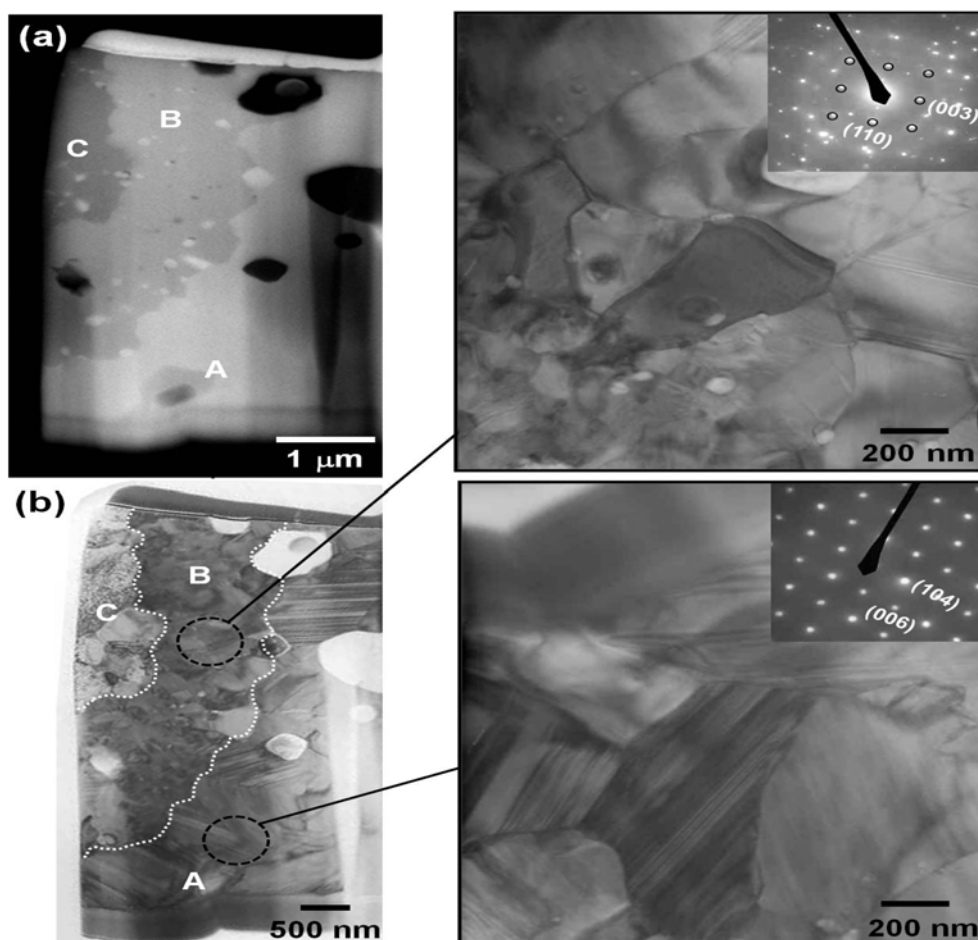


Fig. 5. Results of the microstructural analysis of the R-D processed powder cross sections by the FIB and TEM analysis: (a) preparation of the TEM sample by the FIB technique, (b) TEM micrographs.

formation and growth of SmFe intermetallics are controlled by the reaction temperature and mixing homogeneity as well as the initial powder size [2, 9]. In this respect, considering the characteristics of the initial powder sample in terms of mixing homogeneity and powder size in this study, the microstructure of Fig. 2 can be interpreted as follows. The initial powder mixture was in the form of several tens of micrometer Fe nanopowder agglomerates that were covered with a mixture of Sm_2O_3 and CaH_2 nanopowders. During the annealing process, not only the diffusion reaction but also the sintering of Fe nanopowder inside a large agglomerated powder proceeds simultaneously. In particular, the latter sintering process might occur much earlier at a lower temperature of about 500 °C before the diffusion reaction occurs [18]. Accordingly, the densified microstructure of Fe nanopowders is formed in the center zone with accompanying pore elimination from the center outside the surface during the subsequent diffusion reaction for the formation of interfacial layers. In general, pores are coarsening and accumulated favorably at the interfacial region during migration for the elimination process [19]. The microstructure in Fig. 4 supports this argument. It might also be explained by the Kirkendall

effect [20] in that the pore can be formed by an asymmetrical diffusion reaction between Sm and Fe.

To investigate the crystal structure and microstructure of two intermetallic layers, a TEM study was carried out on the selected region of the cross sectioned surface of the same sample as shown above in Fig. 4b (white line and arrow) using the FIB technique. As depicted in Fig. 5a, the TEM sample taken by the FIB treatment includes three phases of 'A', 'B', and 'C'. Fig. 5b reveals the microstructure and the crystal structure of the reaction phases. It is estimated that the 'A' and 'B' phases unanimously have a similar grain size of 400–800 nm. The SAED patterns identified that the 'A' and 'B' phases are SmFe_3 and $\text{Sm}_2\text{Fe}_{17}$, respectively. This result exactly matches with the phase identifications by XRD (Fig. 3c) and EDS analysis (Fig. 4c). In particular, SAED pattern analysis identified that the crystal structure of the 'B' phase is a rhombohedral structure which corresponds to the $\text{Sm}_2\text{Fe}_{17}$ structure [15]. This $\text{Sm}_2\text{Fe}_{17}$ phase of about 3 μm thick layers consists of several hundred nanograins. These results give an implication that nanoscale $\text{Sm}_2\text{Fe}_{17}$ powder can be synthesized by controlling the diffusion depth using well-dispersed Fe nanopowders.

Conclusions

We reported on the fabrication of nanostructured SmFe intermetallic compounds by the R-D process for a mixture of ball-milled Sm_2O_3 - CaH_2 powders and Fe nanopowders. The SmFe intermetallic phases of $\text{Sm}_2\text{Fe}_{17}$ and SmFe_3 were effectively formed in a switched gas atmosphere from Ar-5 vol.% H_2 to a vacuum atmosphere at 800 °C. The low hydrogen content reducing atmosphere not only enhanced the formation of Sm into SmH_2 but also suppressed the decomposition into the Sm atoms which participate in inter-diffusion with Fe. A subsequent switching atmosphere enhanced the decomposition of SmH_2 and the subsequent diffusion reaction between the Sm and Fe nanopowders, forming two intermetallic phases of $\text{Sm}_2\text{Fe}_{17}$ and SmFe_3 . The $\text{Sm}_2\text{Fe}_{17}$ phase was identified having a rhombohedral $\text{Th}_2\text{Zn}_{17}$ -type (2:17 R) structure with a grain size of 400-800 nm. This result indicates that nanoscale $\text{Sm}_2\text{Fe}_{17}$ powder can be synthesized by controlling the diffusion depth using well-dispersed Fe nanopowders. It also shows the feasibility of making a SmFe intermetallic compounds by a solid state reaction using a powder mixture of Sm_2O_3 - CaH_2 -Fe at low temperature.

References

1. J.M.D. Coey, H. Sun, *J. Magn. Mater.* 87 (1990) L251-L254.
2. J.C. Boareto, J. Soyama, M.D.V. Felisberto, R. Hesse, A.V. A. Pinto, T.R. Taylor, P.A.P. Wendhausen, *Mater. Sci. Forum* 534-536 (2007) 1365-1368.
3. C.N. Christodoulou, T. Takeshita, *J. Alloys Compd.* 202 (1993) 173-182.
4. H. Oda, K. Kondo, H. Uchida, Y. Matsumura, *Jpn. J. Appl. Phys.* 34 (1995) L35-L37.
5. T. Saito, M. Fukui, H. Takeishi, *Scripta Mater.* 53 (2005) 1117-1121.
6. N. Imaoka, T. Iriyama, S. Itoh, A. Okamoto, T. Katsumata, *J. Alloys Compd.* 222 (1995) 73-77.
7. R.E. Cech, U.S. Patent 3, 748, 193. (1973).
8. M.Z. Su, S.F. Liu, X.L. Quian, J.H. Lin, *J. Alloys Compd.* 249 (1997) 229-233.
9. J.C. Yun, G.Y. Lee, J.S. Lee, *Kor. J. Met. Mater.* 48 (2010) 995-1002.
10. S.S. Jung, J.S. Lee, *Mater. Trans.* 50 (2009) 2270-2276.
11. N. Datta, S. Chatterji, J.W. Jeffery, A.L. Mackay, *Min. Mag.* 37 (1969) 250-252.
12. M. Zinkevich, N. Mattern, A. Handstein, O. Gutfleisch, *J. Alloys Compd.* 339 (2002) 118-139.
13. M. Kubis, A. Handstein, B. Gebel, O. Gutfleisch, K.H. Müller, L. Schultz, *J. Alloys Compd.* 308 (2000) 275-279.
14. H. Nakamura, K. Kurihara, T. Tatsuki, S. Sugimoto, M. Okada, M. Homma, *IEEE Translat. J. Magn. Jpn.* 7 (1992) 798-804.
15. H. Fujii, M. Akayama, K. Nakao, K. Tatami, *J. Alloys Compd.* 219 (1995) 10-15.
16. C.J. Smithells, in "Smithells Metals Reference Book" (Butterworth-Heinemann, Oxford, 2004) p.11-295.
17. D. Gengfeng, J. Qingxiu, W. Xiuhong, H. Guirong, Y. Xinyu, *Journal of Rare Earths* 28 (2010) 420-424.
18. Y.H. Zhou, M. Harmelin, J. Bigot, *Scripta Metallurgica* 23 (1989) 1391-1396.
19. R.M. German, in "Sintering theory and Practice" (John Wiley & Sons, Inc., New York, 1996) p. 156.
20. B. Fisher, P.S. Rudman, *Acta Metallurgica* 10 (1962) 37-43.